nature neuroscience

Active flight increases the gain of visual motion processing in *Drosophila*

Gaby Maimon, Andrew D Straw & Michael H Dickinson

We developed a technique for performing whole-cell patch-clamp recordings from genetically identified neurons in behaving *Drosophila*. We focused on the properties of visual interneurons during tethered flight, but this technique generalizes to different cell types and behaviors. We found that the peak-to-peak responses of a class of visual motion–processing interneurons, the vertical-system visual neurons (VS cells), doubled when flies were flying compared with when they were at rest. Thus, the gain of the VS cells is not fixed, but is instead behaviorally flexible and changes with locomotor state. Using voltage clamp, we found that the passive membrane resistance of VS cells was reduced during flight, suggesting that the elevated gain was a result of increased synaptic drive from upstream motion-sensitive inputs. The ability to perform patch-clamp recordings in behaving *Drosophila* promises to help unify the understanding of behavior at the gene, cell and circuit levels.

How does the nervous system transform sensory input into locomotor output? Flies provide an attractive system for studying this question because a large body of work has examined the structure and function of fly sensory systems[1,2], particularly the visual system[3–5], and much is known about the motor signals that drive flight-based locomotion[6]. Prior work has mainly focused on larger dipteran species, but there has been growing interest in the sensory and motor aspects of locomotion in the fruit fly[7], *Drosophila melanogaster*, because of the potential of applying a wide array of genetic tools. In particular, research in *Drosophila* has identified behavioral algorithms that link sensory input to locomotor output[8–10], but determining the neurobiological basis for these algorithms has proven challenging.

Recent advances have made it possible to perform *in vivo* whole-cell patch-clamp recordings from neurons in the adult *Drosophila* brain[11–13]. To date, however, these recordings have only been possible in restrained flies. This is a critical limitation for the study of sensorimotor processing, as central neurons that interpret and integrate sensory signals are likely to respond in a fundamentally different manner during quiescence and active behaviors[14]. Even sensory neurons themselves are known to be influenced by behavioral state in other systems[15–20], but the extent of such modulations in *Drosophila* are not known.

Here we describe a method for performing patch-clamp recordings in tethered, flying *Drosophila*. Our recordings targeted the VS cells of the fly lobula plate, which have been extensively studied in restrained animals[12,21–23] and are thought to estimate self motion during flight so as to facilitate stabilizing reflexes[24]. Our data reveal that VS cells undergo two prominent physiological modulations during flight: a tonic shift in the baseline membrane voltage and a strong boost of visually driven activity. Both of these modulations are likely to change the chemically or electrically mediated synaptic output at the VS-cell terminals. Our results provide the first example, to the best of our knowledge, of patch-clamp recordings in behaving *Drosophila* and indicate that one of the most commonly studied set of visual interneurons is strongly modulated by flight. Our method highlights the importance of studying visual neurons not only in the context of naturalistic sensory input, but also in the context of ethologically relevant locomotory output.

RESULTS

We manufactured a custom stage that allowed us to perfuse the fly's brain with oxygenated saline while the rest of the fly's body remained dry and unconstrained, conditions that permitted tethered-flight behavior (Online Methods and **Fig. 1a**). We attached a fly to this stage under cold anesthesia, removed a patch of cuticle overlying the brain, breached the neural lamella and perineurial sheath with locally applied collagenase (0.5 mg ml^{-1}, <1 µl) and mechanical manipulation, and targeted neuronal cell bodies expressing green fluorescent protein (GFP) with a patch electrode (Online Methods). Once the whole-cell configuration was achieved, we presented a brief air puff to initiate flight and interrupted the wing-stroke plane with a small piece of tissue paper to terminate flight. In some trials, flies would stop flying spontaneously, in which case we would quickly restart flight with additional air puffs. The fly was illuminated with infrared light-emitting diodes (LEDs) at a wavelength that is not visible to the *Drosophila* visual system (880 nm). We registered periods of flight and nonflight with either an infrared sensor that measured the oscillatory changes in light intensity generated by the beating wings or with an infrared-sensitive camera that could visualize the wing stroke envelope from below the fly (Online Methods and **Fig. 1a**).

Our recordings targeted the large tangential neurons of the vertical system (VS cells) in the lobula plate, a higher visual-processing center in flies[3,5,25] (**Fig. 1b**,**c**). Neurons VS1 through VS6 are identifiable across individuals[12,22] and we typically filled neurons with either

Divisions of Biology and Engineering and Applied Sciences, California Institute of Technology, Pasadena, California, USA. Correspondence should be addressed to G.M. (maimon@caltech.edu).

Received 8 September 2009; accepted 28 December 2009; published online 14 February 2010; doi:10.1038/nn.2492

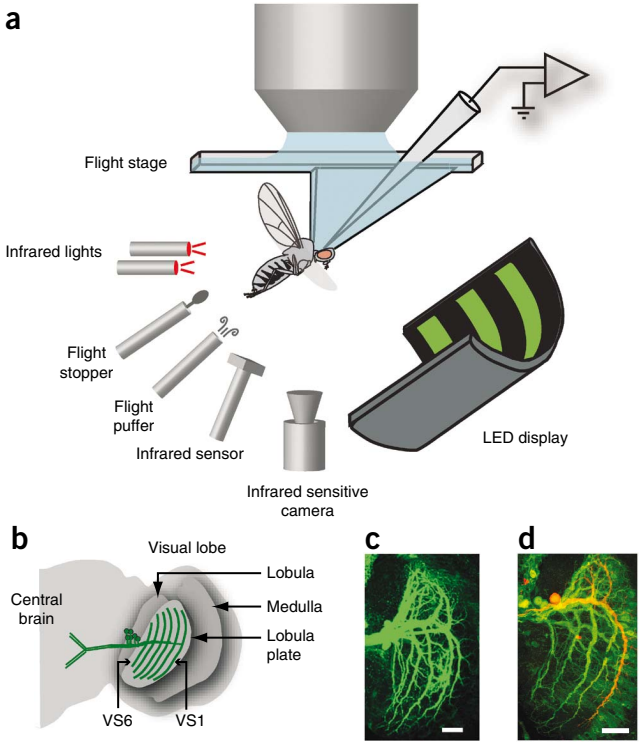

Figure 1 Patch-clamp recordings in tethered, flying *Drosophila*. (**a**) Apparatus. A schematic cutaway of the flight stage is shown. (**b**) Cartoon of the right side of the fly's brain with VS cells highlighted in green. (**c**) Immuno-amplified GFP signal in a fly expressing GFP driven by the *Gal4-3a* promoter (maximal *z* projection of a confocal stack). Only the lobula plate is shown. Scale bar represents 20 µm. (**d**) Immuno-amplified GFP signal (green) and a recorded, biocytin-filled VS1 neuron (red; maximal *z* projection of a two-photon stack). Scale bar is approximately 20 µm.

biocytin or Alexa568 to confirm cell identity after each experiment (Online Methods and **Fig. 1d**). VS cells are thought to primarily signal using graded changes in membrane voltage (V_m), although they do have voltage-gated Na^+ conductances that can generate small-amplitude spikelets and, occasionally, large action potentials[12,26,27]. These visual interneurons respond best to optic-flow stimuli generated by rotations of the fly's body along various azimuthal axes, with a different preferred axis for each VS cell[24]. For example, VS1 depolarizes to downward motion in front of the fly and (less strongly to) upward motion behind the fly, such that this cell probably responds best to a nose-up rotational pitch in free flight. In *Drosophila*, VS1–4 generally depolarize to downward motion in the ispilateral frontal visual field[12] and our experiments therefore focused on frontal, wide-field stimuli presented to these four cell types. VS5 and VS6 receive their feedforward visual inputs from peripheral parts of the visual world that were beyond the edge of our hemispherical visual display and we therefore do not present data from VS5 and VS6.

After removing the perineurial sheath over the recording area, the flies' natural extracellular brain fluid was exchanged with our bath medium. This exchange is likely to alter the concentrations of ions, transmitters and modulators in the brain, which could affect the flies' capacity to produce normal visually guided behavior. To determine whether the flies' behavior was robust in our preparation, we measured an optomotor response, during physiological recording sessions, by presenting the flies with moving gratings and monitoring their wing-stroke amplitudes (**Fig. 2a**,**b**). We estimated stroke amplitudes in real time by analyzing video footage of the flies (Online Methods, **Supplementary Fig. 1** and **Supplementary Video 1**). The image-analysis algorithm that we used is distinct from past approaches for measuring flight steering responses[28,29] and the analysis algorithm could be modified in future experiments for measuring other behaviors, such as tethered walking, grooming and take-off. When flies viewed an upward moving grating, which simulates the visual stimulus generated by a drop in altitude or a nose-down pitch during free flight, the flies responded with a gradual increase in wing stroke amplitude of both wings (**Fig. 2c**). When the flies viewed a downward moving grating, which simulates an increase in altitude or nose-up pitch, the flies responded with a slight decrease in wing stroke amplitude (**Fig. 2c**). This asymmetry, in which the response to downward motion was weaker than the response to upward motion, was consistent across the flies and appeared to reflect a nonlinearity in the flight control system; stronger downward stimuli commonly induced a cessation of flight rather than a further decrease in wing stroke amplitude, suggesting that flies possess a stroke-amplitude limit below which their flight motor cannot operate. These optomotor responses are consistent with previous results from intact, tethered flies[30,31].

To test whether behavioral state influences VS cell physiology, we compared responses to wide-field moving gratings during periods of flight and nonflight. We determined the responses of a single VS cell (from the right lobula plate) to a grating stimulus, which, on any given presentation, moved in one of eight possible directions (**Fig. 3a**).

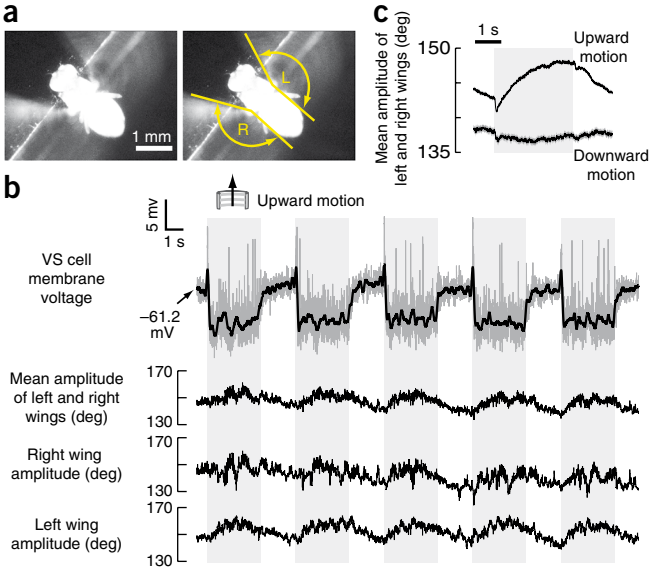

Figure 2 Behavioral measurements of wing stroke amplitude during tethered flight. (**a**) Wing stroke envelopes were visible in an infrared image from below the fly (left). Using image analysis, we extracted the maximum stroke amplitude of the two wings in each frame (yellow lines; Online Methods). (**b**) Sample traces of simultaneously acquired wing stroke amplitude measurements and a whole-cell patch-clamp recording. Black membrane voltage trace shows a digitally low pass–filtered version of the gray trace (fourth-order Butterworth, 25-Hz cutoff). (**c**) Mean stroke-amplitude responses to down and up moving gratings. These traces are drawn from the dataset in **Figure 6** (45 flies were tested: 42 with both up and down motion, 1 with only down motion and 2 with only up motion). We only included cases in which the flies flew continuously throughout the trial. We averaged 752 traces for up motion and 293 traces for down motion.

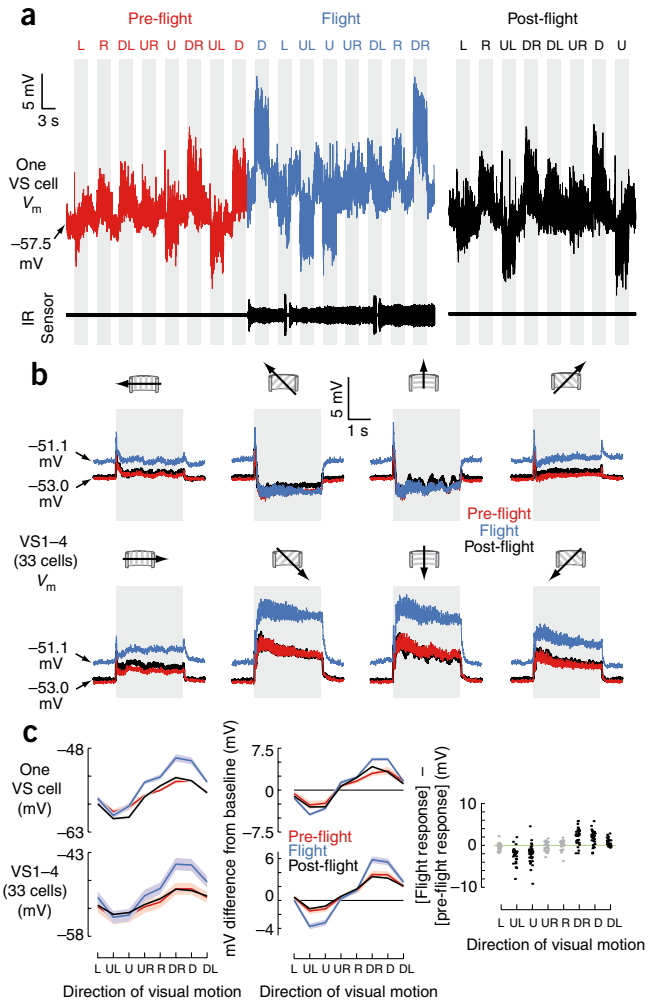

Figure 3 Visual responses of VS cells are boosted and the resting potential depolarizes during flight. (**a**) Membrane voltage of a VS cell before, during and after flight. This fly stopped flying twice during the flight epoch shown (breaks in the infrared sensor trace), but immediately restarted each time following delivery of an air puff. The post-flight trace shares the same *y* axis scale and offset as the pre-flight/flight trace. D, down; DL, down-left; DR, down-right; L, left; R, right; U, up; UL, up-left; UR, up-right. (**b**) Mean responses of 33 VS neurons from the right lobula plate to the eight directions of grating motion. Note that the membrane potential before (red) and after (black) flight was quite similar, even though these data were collected ≥8 min apart. This stability of the membrane potential was typical of our recordings. (**c**) Tuning curves. Left, the mean voltage (±s.e.m.) for the eight stimuli in the final 2.8 s of the stimulus presentation period for the single cell from **a** (top) and for the population (bottom). Middle, baseline-subtracted mean voltage responses to the eight stimuli (±s.e.m.). Standard errors of post-flight curves were very similar in magnitude to pre-flight curves and are not shown for clarity. Right, difference between baseline-subtracted responses in flight and pre-flight conditions, one point per cell, per stimulus. Distributions whose mean significantly differs from zero are shown in black (*t* test, Bonferroni-corrected threshold of $P < 0.01$).

We pseudo-randomly shuffled the presentation order for each block of eight stimuli. Both during nonflight and flight, this cell depolarized most strongly to down and down-right motion, and hyperpolarized most prominently to up and up-left motion. However, visually driven responses were larger during flight than nonflight in both the depolarizing and hyperpolarizing direction. In addition, the cell exhibited a tonic 1–2-mV depolarization of its baseline resting potential in flight compared with nonflight, which was observable in the epochs between visual stimuli (VS-cell responses at a higher time resolution are shown in **Supplementary Fig. 2**).

The flight-induced effects on the baseline potential and visually driven activity were evident in population-averaged responses from 33 VS cells (**Fig. 3b**). We measured the mean V_m in the final 2.8 s of the 3-s stimulus-presentation period and plotted a tuning curve of this voltage for the example cell and for the population (**Fig. 3c**). We also determined the baseline-subtracted tuning curves (**Fig. 3c**), in which, for each trial, we subtracted the mean voltage in the final 1 s of the preceding intertrial period from the mean voltage recorded during stimulus presentation.

Baseline-subtracted responses to down-right, down, and down-left stimuli were significantly larger during flight versus nonflight (*t* test; down-right, $P = 5.9 \times 10^{-7}$; down, $P = 5.3 \times 10^{-7}$; down-left, $P = 5.9 \times 10^{-4}$; **Fig. 3c**), with an average V_m of +3.71, +3.67 and +2.05 mV during nonflight and +5.84, +5.50 and +2.62 mV during flight, respectively. Baseline-subtracted, hyperpolarizing responses to up-left and up stimuli were also significantly larger during flight than during nonflight (*t* test; up-left, $P = 8.1 \times 10^{-8}$; up, $P = 3.1 \times 10^{-5}$; **Fig. 3c**), with an average V_m of −1.50 and −1.20 mV during nonflight and −3.73 and −3.18 mV during flight, respectively. Responses to the other three motion directions were not significantly different between flight and nonflight (*t* test, Bonferroni corrected threshold of $P < 0.01$; left, $P = 0.01$; up-right, $P = 0.24$; right, $P = 0.69$). It should be noted that these potentials were recorded with a patch electrode on a soma that was connected to the cell's dendrites by a fine neurite. The changes in V_m in response to visual motion and flight are expected to be much larger in the terminals of VS cells.

The two effects of flight, baseline depolarization and boosted visual responses, could have the same biophysical origin. For example, a reduced K^+ conductance could bias the resting potential to be more positive and increase the input resistance of the cell[32], yielding larger visual responses. To test for a change in input resistance, we measured steady-state whole-cell currents in response to a series of voltage steps during flight and nonflight (**Fig. 4a**). Because of space-clamp limitations, we commonly observed unclamped action potentials in the current traces (**Fig. 4a**), but these did not corrupt measurements of steady-state currents taken in the final 25 ms of each 100-ms voltage pulse. We estimated the passive membrane resistance from the slope of the steady-state current-voltage relationship observed at hyperpolarized voltages (Online Methods and **Fig. 4b**). Rather than increase during flight, the passive membrane resistance (R_m) of VS cells dropped by an average of 7.3%, from a mean of 218 MΩ before flight to a mean of 202 MΩ during flight, recovering to a slightly higher value of 227 MΩ after flight (**Fig. 4c**). All 12 cells tested showed a decrease in passive R_m between pre-flight and flight conditions, a drop that was statistically significant across the population (*t* test, $P = 0.0018$; **Fig. 4c**). These observed changes in input resistance at the soma are again likely to underestimate the actual modifications taking place at the input and output regions of the cells.

Without further work we cannot conclusively determine whether the reduced input resistance arises from the opening of postsynaptic receptors, gap junctions, voltage-gated ion channels or other ion channels. However, during flight compared with nonflight, we did observe a significant rise in the variance of both the baseline V_m trace (*t* test, $P = 8.4 \times 10^{-12}$; **Fig. 4d,e**) and voltage-clamp current traces at hyperpolarized potentials (*t* test, $P = 3.2 \times 10^{-5}$; **Fig. 4f,g**), where most voltage-gated ion channels are expected to be closed. These observations suggest, but do not prove, that VS cells receive a barrage of depolarizing synaptic inputs during flight that cause the baseline shift.

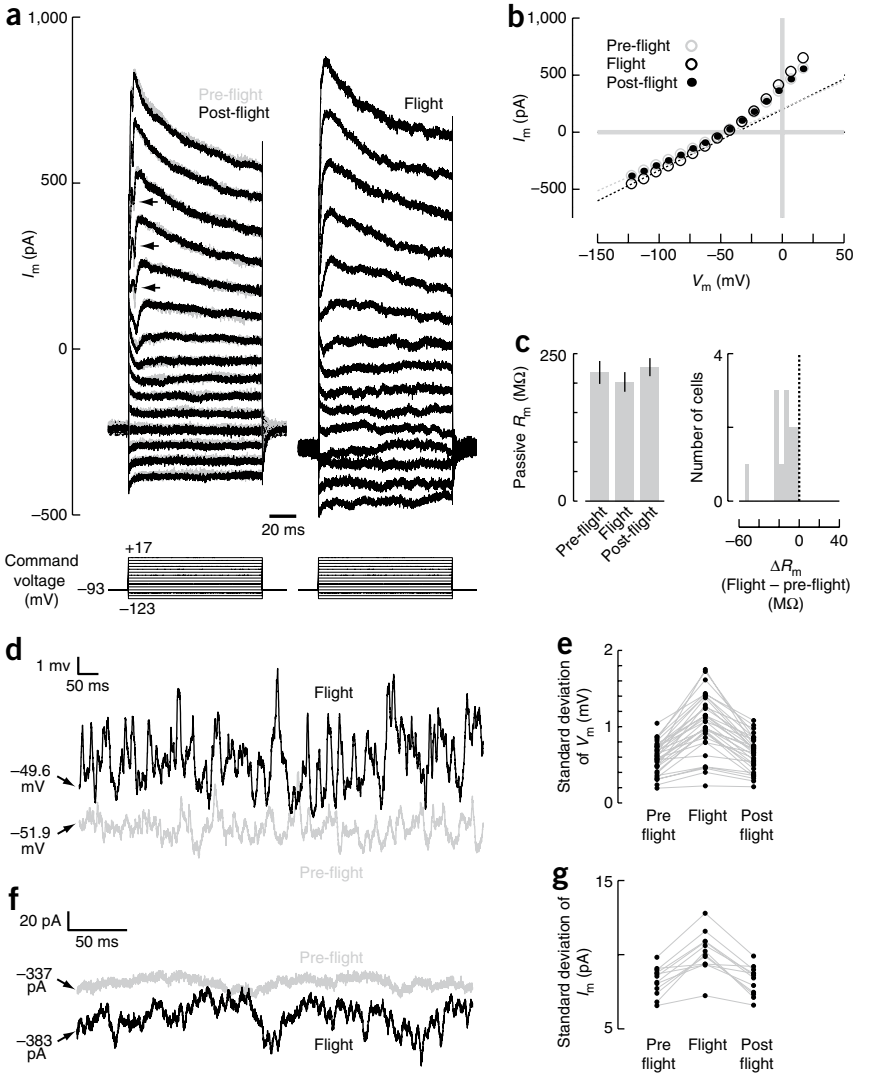

Figure 4 During flight, passive membrane-resistance decreases and membrane voltage and current fluctuations increase. (**a**) Signal-averaged current traces measured before flight ($n = 3$ traces per voltage step), during flight ($n = 3$) and after flight ($n = 4$) in response to the family of voltage steps shown below (Online Methods). Arrows indicate unclamped action potentials. (**b**) Current-voltage (*I-V*) curves generated from the data in **a**. We averaged the current and voltage traces over the final 25 ms to generate the steady-state values that are plotted. We fit a line based on the four most hyperpolarized voltage steps to generate estimates of the passive membrane resistance (1/slope = R_m) for pre-flight, flight and post-flight conditions. For clarity, only fits for pre-flight and flight are shown (dotted lines). This cell's R_m was 209 MΩ pre-flight, 187 MΩ during flight and 209 MΩ post-flight. (**c**) Left, mean (±s.e.m.) membrane resistances for pre-flight, flight and post-flight epochs ($n = 12$ cells). Right, distribution of the cell-by-cell differences in R_m between flight and pre-flight conditions. (**d**) Sample baseline V_m traces from a single neuron during flight and non-flight. (**e**) Using the dataset from **Figure 6**, we measured the s.d. of V_m in the 1-s baseline period preceding each stimulus and compared this value between pre-flight, flight and post-flight epochs (right). We required that the fly was flying for the entire duration of the 1-s baseline period, 3-s stimulus period and 1-s post-stimulus period for an s.d. measurement to be taken. At least one such trial was procured from 40 of the 45 cells. (**f**) Sample current traces from a single neuron held at −93 mV. (**g**) Mean s.d. (±s.e.m.) of current traces before, during and after flight. For each cell, we measured the s.d. of I_m in the final 25 ms of hyperpolarized voltage steps (−123 to −73 mV) and averaged these values in each condition ($n = 12$ cells).

Note that the baseline shift during flight was not observed in other neuron types and was not a mechanical artifact (**Fig. 5**).

A drop in input resistance should, all things being equal, decrease the size of visually driven potentials recorded at the soma. Thus, the observed increase of visually driven responses during flight (**Fig. 3**) is most likely a result of an additional effect. To further test whether the baseline shift and visual boost were the result of identical or separate mechanisms, we examined their time course at the beginning and end of flight. We repeatedly presented a downward moving grating (**Fig. 6a**) or an upward moving grating (**Fig. 6b**) and induced the animals to fly for 40–400 s (8–80 stimuli, Online Methods). We quantified the strength of the visual response by averaging V_m in the final 2.8 s of each 3-s stimulus-presentation period and subtracted from this the mean V_m in the final 1 s of the preceding intertrial period (**Fig. 6c**). We quantified the baseline shift simply by noting the mean V_m in the final 1 s of each inter-trial period (**Fig. 6c**). Our results indicate that although both the visual boost and baseline shift were immediately evident at the onset of flight, the two effects had very different recovery time courses following the cessation of flight. The baseline shift recovered immediately, whereas the visual boost, for both depolarizing and hyperpolarizing stimuli, recovered in an exponential-like manner with a time constant of 5–10 s. Qualitatively different recovery time courses for the baseline shift and visual boost support the hypothesis that the two effects are caused by separate biophysical mechanisms.

In most experiments, we applied brief air puffs to the flies to restart flight, at an average rate of ~0.2 Hz (**Fig. 6a**,**b**). One possibility is that the observed physiological effects were caused by the externally applied air puffs and not the fly's flight status *per se*. To test this possibility, we examined data from cases in which the flies flew continuously, with no air puff, for at least 35 s (**Supplementary Fig. 3**). We observed no decline of the baseline shift or visual boost over these extended periods of continuous flight, indicating that both effects had not been caused by the air puffs.

DISCUSSION

Here we describe a method for recording from genetically identified neurons in flying *Drosophila* (**Fig. 1**). Notably, the flies' optomotor responses are intact in this preparation (**Fig. 2**). Although we did not observe a strong correlation between the magnitude of neuronal and behavioral responses on a stimulus-by-stimulus basis in these experiments (data not shown; for example, see **Fig. 2**), future experiments employing novel behaviors and stimuli, as well as activation and inactivation protocols using current injection, are expected to

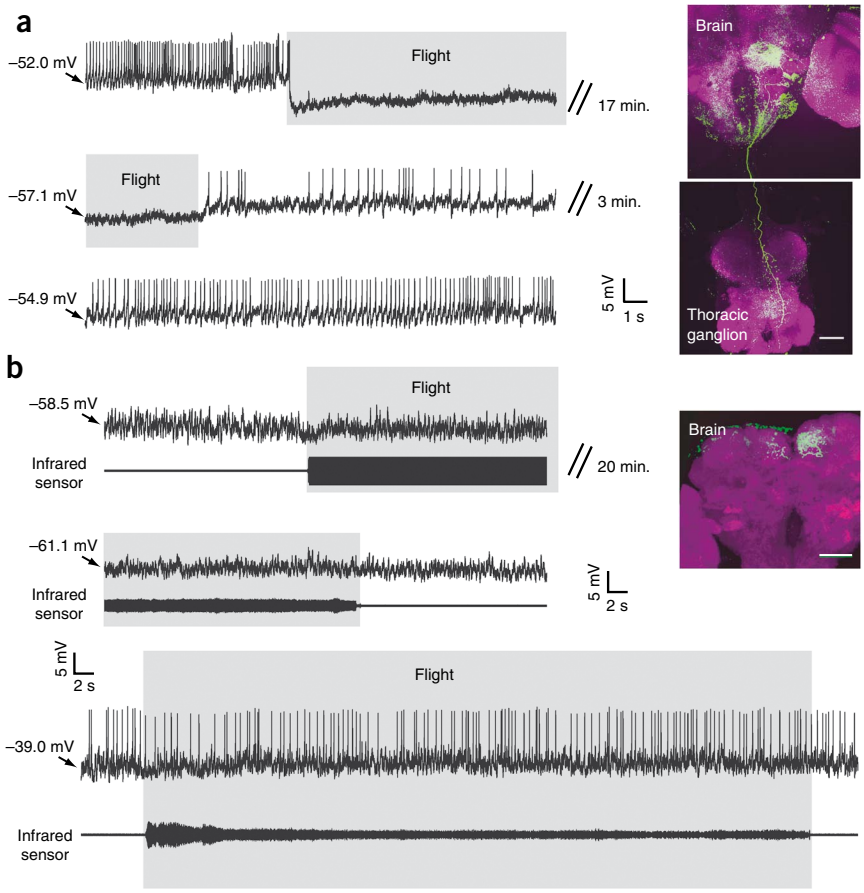

Figure 5 Other neurons in the central brain are not depolarized during flight. (**a**) Membrane voltage of a descending interneuron before, during and after flight. // indicates a break in the trace of the specified duration. This fly flew continuously for 17 min and the cell was tonically hyperpolarized during flight. The flight-induced hyperpolarization eliminated all spiking activity. The observation that some cells hyperpolarize with flight thus acts as a control to show that the tonic depolarization of VS cells is unlikely to be a trivial property of all brain cells during flight (or a mechanical artifact), but is instead a specific property of VS-cell circuitry. Biocytin fill (green) and nc-82 neuropil stain (magenta) are shown on the right. This cell sent its axon down to the thoracic ganglion (maximal intensity confocal projection). Scale bar represents 50 μm. (**b**) Membrane voltage of a cell that did not show a strong modulation as a result of flight. Top, cell at its natural resting potential of approximately –60 mV, at which it did not fire spontaneous action potentials. This cell's membrane voltage was not strongly altered by flight. The large, saturating infrared sensor signal at the start of flight was a result of the sensor's gain set slightly too high; we lowered the gain mid-way through the flight bout. Bottom, we injected current to depolarize the neuron by 20 mV at the soma, which caused the cell to spike at ~2 Hz. When we induced flight, we observed no obvious change in spike rate. Biocytin fill (green) and nc-82 neuropil stain (magenta) are shown on the right (maximal intensity confocal projection). Scale bar represents 50 μm.

greatly clarify VS-cell function during flight. The membrane voltage of VS cells was tonically depolarized during flight and visual responses were strongly boosted (**Figs. 3** and **6**). The results of our voltage-clamp experiments suggest that VS cells receive an increased barrage of synaptic input when flies fly (**Fig. 4**), which leads to the baseline depolarization. Boosted visual responses are probably a result of a separate mechanism, as these recover more slowly than the baseline shift after the cessation of flight (**Fig. 6**).

Advances in visual-display technology should allow one to use a panoramic screen with this preparation in the future. However, a current limitation is that visual stimuli are only presented in the frontal visual field. This is an important consideration for wide-field stimuli designed to mimic the patterns of optic flow generated by a locomoting animal. For example, a fly that rises in altitude experiences downward motion in the front and rear visual fields, whereas an animal undergoing a nose-up pitch experiences downward motion frontally, but upward motion in the rear. Thus, the frontal downward stimulus that we presented in these experiments was behaviorally ambiguous and it is possible that the asymmetry in observed wing stroke responses to upward and downward moving gratings (**Fig. 2c**) was partly the result of the limited spatial extent of our visual stimulus. At the neuronal level, our frontal display strongly stimulated the feedforward visual inputs to VS1–4, which were clearly boosted during flight. VS5–6, on the other hand, had their feedforward inputs beyond the extent of our display, and were therefore stimulated mainly through lateral connectivity. As a consequence, the observed effects of flight on the visual responses of VS5–6 were more complex with this setup (data not shown).

Gain changes and matched filters

In blowflies, researchers have mapped the motion-direction selectivity of VS cells at local regions across the retina[24,33]. These measurements have led to the suggestion that VS cells act as matched filters to wide-field optic-flow stimuli generated by rotations of the fly during flight. VS1, for example, prefers downward motion in the frontal visual field and upward motion in the rear visual field, suggesting that this cell is best activated by (that is, acts as a matched-filter for) a nose-up pitch during free flight.

In our experiments, we found that the gain of VS-cell responses to wide-field stimuli is increased during flight. This global gain change could arise from two non–mutually exclusive changes to local receptive-field properties. First and most simply, local direction selectivity across the retina could remain unchanged during flight, but the gain of local responses may be enhanced. Alternatively, local gains might remain unchanged, but local preferred directions could shift during flight so as to better align with our wide-field stimuli and thus strengthen responses. Because we did not comprehensively map the local receptive-field properties of VS cells in flight, we could not definitively distinguish between these possibilities. Note, however, that the population tuning curves in flight and nonflight (**Fig. 3c**) have a similar shape, sharing subtleties such as down-right stimuli being slightly more depolarizing than down stimuli and up-left stimuli being slightly more hyperpolarizing than up stimuli. Such similarities in tuning-curve shapes are more likely to result from a simple gain change in local responses[34] and are less likely to result from a more complex reorganization of the direction-selective properties of the receptive field.

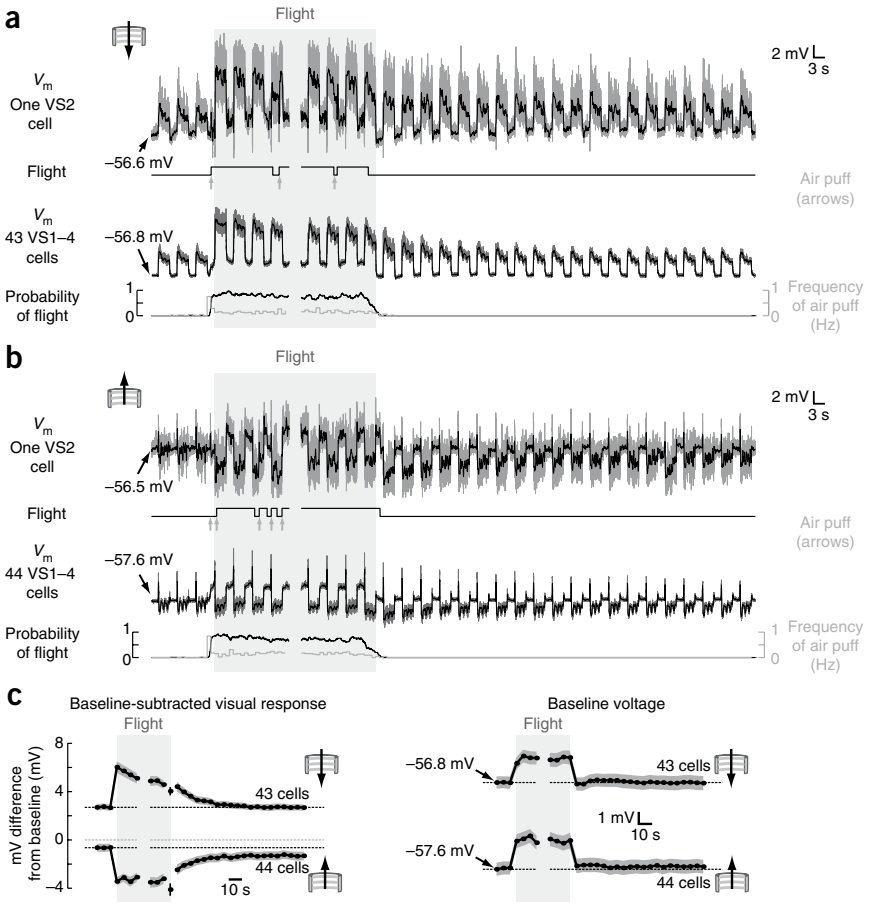

Figure 6 The baseline depolarization and visual-response boost have different recovery dynamics at the cessation of flight. (**a**) Responses of one VS cell (top) and mean responses of a population of 43 VS cells (bottom) to repeated presentations of downward moving grating (3-s stimulus, 2-s intertrial) before, during and after flight. Highlighted in light gray is the flight epoch, beginning with the start of the first grating presentation during flight and terminating with the end of the last grating presentation during flight. Digitally low pass–filtered traces (fourth-order Butterworth, 25-Hz cutoff) are shown in black. Periods of flight and nonflight, as well as the instances of air puffs (gray arrows), are indicated below the single-cell trace. The probability of flies flying (a value of 1 indicates all flies flew 100% of the time in that bin) and the puffing rate are indicated below the population-averaged trace. There is a discontinuity in the *x* axis because different flies flew for different lengths of time between the first four and last four stimuli (Online Methods). (**b**) Data are presented as in **a**, except we repeatedly presented an upward moving grating. The same example neuron is shown in **a** and **b**. (**c**) Quantification of the visual boost and baseline shift over time. For each stimulus, we measured the mean V_m in the final 2.8 s of the stimulus presentation period and subtracted the mean voltage from the 1 s immediately preceding the stimulus. The baseline-subtracted response over time (±s.e.m.) for downward and upward gratings is shown on the left. For the first stimulus presented during flight, we subtracted the baseline voltage following, not preceding, the stimulus; this was necessary because flight initiation was often induced only part way through the preceding intertrial period. For the final stimulus during flight we could not get an accurate estimate of the response strength (isolated black dot) because the flies typically stopped flying on their own at a variable time point in the last stimulus/intertrial period. The mean baseline voltage in the 1 s preceding each stimulus (±s.e.m.) is shown on the right.

A baseline shift and visual boost in VS cells

Although external mechanosensory stimuli (air puffs) were not essential for the observed effects, many mechanosensory sensilla on the antennae, wings and halteres are undoubtedly active in flight. One possibility is that these mechanoreceptors (or downstream neurons) provide input to VS cells during flight, leading to the observed baseline shift or that a central signal that drives active movements of these appendages sends a corollary discharge to the visual system[19]. The observed changes in visual-response gain might be mediated by a neuromodulator released during flight. The *Drosophila* visual lobes, including the lobula plate, are densely innervated by processes of central octopaminergic neurons[35] and it has been shown in blowflies[34] that exogenous application of an octopamine agonist modulates the responses spiking lobula-plate cells in a manner reminiscent of the effects that we observed in VS cells. Octopamine, which has been intimately linked to flight behavior[36,37], might be released onto VS cells (or upstream neurons) and could contribute to the boost of visual responses as well as the baseline shift. Lobula-plate tangential cells also show adaptation of their contrast gain in response to persistent visual input[38] and the change in gain reported here during flight might employ similar mechanisms.

Regardless of the underlying biophysics, the data demonstrate that VS cells respond to visual stimuli much more strongly during flight than nonflight. VS cells therefore do not provide an invariant visual signal, as was originally postulated[25]. The observed gain change may act like a gate, whereby VS cells drive downstream neurons effectively only when flies are flying. It would also save the animal energy to keep responses at a minimum during nonflight[39], if VS cells are not in use. Alternatively, these neurons may still contribute to behaviors on the ground, but with different roles than in flight, requiring lower gain.

Patch-clamp recordings in behaving *Drosophila*

Our technique offers several advantages for the study of sensorimotor processing. One can target genetically identified cell types for recordings, measure optomotor responses in real time, perform stable intracellular measurements in which subthreshold events are discernible, activate or inactivate single neurons with current injection, control the intracellular and extracellular ionic compositions, and perform genetic manipulations in a rapid and flexible manner. Few other preparations for behavioral physiology share these features[40]. Although our experiments focused on whole-cell recordings, in which the internal contents of the cell were gradually replaced with the pipette solution, it is also feasible to record from spiking neurons in our preparation with the loose-patch technique (**Supplementary Fig. 4**), where the intracellular volume of the cell remains largely unaltered.

Drosophila has long been a model for studying the genetic basis of behavior[41]. It has also been possible to link genetic manipulations

in *Drosophila* to electrophysiological effects in peripheral neurons, synapses, and muscles, thereby explaining many behavioral phenotypes. However, it has proven more difficult to make this link when genetic manipulations have their effect deeper in the CNS. The ability to patch-clamp brain neurons in behaving *Drosophila* opens the door for understanding the cellular basis of behavioral phenotypes that arise from changes to central-brain processing[42,43]. Our method may therefore provide an important link between genetics and higher-order behaviors. In particular, our preparation provides an immediate platform for studying the roles of central neurons, such as cells of the optic foci of the lateral protocerebrum[44], descending interneurons and central complex neurons, whose behavioral functions remain largely unknown. The combination of genetic tools available for *Drosophila* with behavioral patch-clamp physiology establishes a new testing ground for discovering the cellular principles of sensorimotor processing and integrative brain function.

METHODS

Methods and any associated references are available in the online version of the paper at http://www.nature.com/natureneuroscience/.

Note: Supplementary information is available on the Nature Neuroscience website.

ACKNOWLEDGMENTS

We thank J. Assad, V. Bhandawat, G. Card, C. Chiu, M. Do, T. Herrington, W. Korff, G. Laurent, M. Murthy, P. Polidoro, G. Turner and R. Wilson for helpful discussion, comments and aid in developing the preparation. We are grateful to L. Luo for the Gal4-3a fly line. This work was supported by a National Science Foundation Frontiers in Integrative Biological Research 0623527 award (M.H.D.) and a Caltech Della Martin fellowship (G.M.).

AUTHOR CONTRIBUTIONS

G.M., A.D.S. and M.H.D. designed the experiments. G.M. and M.H.D. wrote the paper. G.M. developed the preparation, conducted the experiments and analyzed the data. A.D.S. designed the software and hardware system for tracking wing beat amplitudes in real time.

COMPETING INTERESTS STATEMENT

The authors declare no competing financial interests.

Published online at http://www.nature.com/natureneuroscience/.
Reprints and permissions information is available online at http://www.nature.com/reprintsandpermissions/.

1. Strausfeld, N.J. *Atlas of an Insect Brain* 214 (Springer-Verlag, 1976).
2. Taylor, G.K. & Krapp, H.G. Sensory systems and flight stability: what do insects measure and why? in *Insect Mechanics and Control: Advances in Insect Physiology,* Vol. 34 (eds. Casas, J. & Simpson, S.J.) 231–316 (Academic Press, London, 2007).
3. Borst, A. & Haag, J. Neural networks in the cockpit of the fly. *J. Comp. Physiol. A Neuroethol. Sens. Neural Behav. Physiol.* **188**, 419–437 (2002).
4. Hausen, K. Decoding of retinal image flow in insects. *Rev. Oculomot. Res.* **5**, 203–235 (1993).
5. Krapp, H.G. & Wicklein, M. in *The Senses: a Comprehensive Reference* (eds. Basbaum, A.I., Kaneko, A. & Shepherd, G.M.) 131–204 (Academic Press, London, 2008).
6. Balint, C.N. & Dickinson, M.H. The correlation between wing kinematics and steering muscle activity in the blowfly *Calliphora vicina*. *J. Exp. Biol.* **204**, 4213–4226 (2001).
7. Frye, M.A. in *Avances in Invertebrate Neurobiology* (eds Greenspan, R. & North, G.) (Cold Spring Harbor Laboratory Press, Cold Spring Harbor, New York, 2007).
8. Gotz, K.G. Flight control in *Drosophila* by visual perception of motion. *Kybernetik* **6**, 199–208 (1968).
9. Tammero, L.F. & Dickinson, M.H. Collision-avoidance and landing responses are mediated by separate pathways in the fruit fly, *Drosophila melanogaster*. *J. Exp. Biol.* **205**, 2785–2798 (2002).
10. Budick, S.A. & Dickinson, M.H. Free-flight responses of *Drosophila melanogaster* to attractive odors. *J. Exp. Biol.* **209**, 3001–3017 (2006).
11. Wilson, R.I., Turner, G.C. & Laurent, G. Transformation of olfactory representations in the *Drosophila* antennal lobe. *Science* **303**, 366–370 (2004).
12. Joesch, M., Plett, J., Borst, A. & Reiff, D.F. Response properties of motion-sensitive visual interneurons in the lobula plate of *Drosophila melanogaster*. *Curr. Biol.* **18**, 368–374 (2008).
13. Turner, G.C., Bazhenov, M. & Laurent, G. Olfactory representations by *Drosophila* mushroom body neurons. *J. Neurophysiol.* **99**, 734–746 (2008).
14. Ramirez, J.M. & Pearson, K.G. Alteration of bursting properties in interneurons during locust flight. *J. Neurophysiol.* **70**, 2148–2160 (1993).
15. Treue, S. & Maunsell, J.H. Attentional modulation of visual motion processing in cortical areas MT and MST. *Nature* **382**, 539–541 (1996).
16. Schmidt, M.F. & Konishi, M. Gating of auditory responses in the vocal control system of awake songbirds. *Nat. Neurosci.* **1**, 513–518 (1998).
17. Rowell, C.H.F. Variable responsiveness of a visual interneurone in the free-moving locust and its relation to behaviour and arousal. *J. Exp. Biol.* **55**, 727–747 (1971).
18. Rind, F.C., Santer, R.D. & Wright, G.A. Arousal facilitates collision avoidance mediated by a looming sensitive visual neuron in a flying locust. *J. Neurophysiol.* **100**, 670–680 (2008).
19. Rosner, R., Egelhaaf, M. & Warzecha, A.K. Behavioural state affects motion-sensitive neurones in the fly visual system. *J. Exp. Biol.* **213**, 331–338 (2010).
20. Tomioka, K. & Yamaguchi, T. Response modification of cricket sensory interneurons during flight. *Zoolog. Sci.* **1**, 169–186 (1984).
21. Hengstenberg, R. Common visual response properties of giant vertical cells in the lobula plate of the blowfly *Calliphora*. *J. Comp. Physiol. A. Neuroethol. Sens. Neural Behav. Physiol.* **149**, 179–193 (1982).
22. Scott, E.K., Raabe, T. & Luo, L. Structure of the vertical and horizontal system neurons of the lobula plate in *Drosophila*. *J. Comp. Physiol.* **454**, 470–481 (2002).
23. Haag, J. & Borst, A. Neural mechanism underlying complex receptive field properties of motion-sensitive interneurons. *Nat. Neurosci.* **7**, 628–634 (2004).
24. Krapp, H.G. & Hengstenberg, R. Estimation of self-motion by optic flow processing in single visual interneurons. *Nature* **384**, 463–466 (1996).
25. Hausen, K. The lobula-complex of the fly: structure, function and significance in visual behavior. in *Photoreception and Vision in Invertebrates* (ed. Ali, M.A.) (Plenum Press, New York, 1984).
26. Hengstenberg, R. Spike responses of nonspiking visual inter-neurone. *Nature* **270**, 338–340 (1977).
27. Haag, J., Theunissen, F. & Borst, A. The intrinsic electrophysiological characteristics of fly lobula plate tangential cells. 2. Active membrane properties. *J. Comput. Neurosci.* **4**, 349–369 (1997).
28. Gotz, K.G. Course-control, metabolism and wing interference during ultralong tethered flight in *Drosophila melanogaster*. *J. Exp. Biol.* **128**, 35–46 (1987).
29. Graetzel, C.F., Fry, S.N. & Nelson, B.J. A 6,000-Hz computer vision system for real-time wing beat analysis of *Drosophila*. in *BioRob. The First IEEE/RAS-EMBS Internation Conference on Biomdeical Robotics and Biomechatronics* 1–6 (Institute of Electrical and Electronics Engineers, Pisa, Italy, 2006).
30. Heisenberg, M., Wonneberger, R. & Wolf, R. Optomotor-blind^{H31}—a *Drosophila* mutant of the lobula plate giant neurons. *J. Comp. Physiol. A. Neuroethol. Sens. Neural Behav. Physiol.* **124**, 287–296 (1978).
31. Gordon, S. & Dickinson, M.H. Role of calcium in the regulation of mechanical power in insect flight. *Proc. Natl. Acad. Sci. USA* **103**, 4311–4315 (2006).
32. North, R.A. & Uchimura, N. 5-Hydroxytryptamine acts at 5-HT2 receptors to decrease potassium conductance in rat nucleus accumbens neurones. *J. Physiol. (Lond.)* **417**, 1–12 (1989).
33. Krapp, H.G., Hengstenberg, B. & Hengstenberg, R. Dendritic structure and receptive-field organization of optic flow processing interneurons in the fly. *J. Neurophysiol.* **79**, 1902–1917 (1998).
34. Longden, K.D. & Krapp, H.G. State-dependent performance of optic-flow processing interneurons. *J. Neurophysiol.* **102**, 3606–3618 (2009).
35. Busch, S., Selcho, M., Ito, K. & Tanimoto, H. A map of octopaminergic neurons in the *Drosophila* brain. *J. Comp. Neurol.* **513**, 643–667 (2009).
36. Orchard, I., Ramirez, J.M. & Lange, A.B. A multifunctional role for octopamine in locust flight. *Annu. Rev. Entomol.* **38**, 227–249 (1993).
37. Brembs, B., Christiansen, F., Pfluger, H.J. & Duch, C. Flight initiation and maintenance deficits in flies with genetically altered biogenic amine levels. *J. Neurosci.* **27**, 11122–11131 (2007).
38. Harris, R.A., O'Carroll, D.C. & Laughlin, S.B. Contrast gain reduction in fly motion adaptation. *Neuron* **28**, 595–606 (2000).
39. Niven, J.E. & Laughlin, S.B. Energy limitation as a selective pressure on the evolution of sensory systems. *J. Exp. Biol.* **211**, 1792–1804 (2008).
40. Fetcho, J.R., Higashijima, S. & McLean, D.L. Zebrafish and motor control over the last decade. *Brain Res. Rev.* **57**, 86–93 (2008).
41. Benzer, S. Behavioral mutants of *Drosophila* isolated by countercurrent distribution. *Proc. Natl. Acad. Sci. USA* **58**, 1112–1119 (1967).
42. Liu, G. *et al.* Distinct memory traces for two visual features in the *Drosophila* brain. *Nature* **439**, 551–556 (2006).
43. Neuser, K., Triphan, T., Mronz, M., Poeck, B. & Strauss, R. Analysis of a spatial orientation memory in *Drosophila*. *Nature* **453**, 1244–1247 (2008).
44. Strausfeld, N.J., Sinakevitch, I. & Okamura, J.Y. Organization of local interneurons in optic glomeruli of the dipterous visual system and comparisons with the antennal lobes. *Dev. Neurobiol.* **67**, 1267–1288 (2007).

ONLINE METHODS

Flies. We studied 2–3-d-old female *Drosophila melanogaster* derived from the cross of a Gal4-3a driver line[22], which targets the vertical system tangential cells (VS cells) of the lobula plate, and a UAS-2xEGFP responder line (Bloomington). We recorded a few VS cells in wild-type *Drosophila* from our lab stock, descended from 200 wild-caught individuals, and the results were similar to those of the genetic cross (data not shown).

Visual display and stimuli. Each pixel of the LED display[45] subtended a solid angle of ~2.5°, and the full arena subtended ±90° horizontally by ±35° vertically. Our stimuli were full-field square-wave gratings (10 pixels, or approximately 25°, per cycle) that moved at a 1-Hz temporal frequency, which is near the optimal frequency for *Drosophila* VS cells[12]. These stimuli had a nominal Michelson contrast of 1, although reflections may have slightly reduced this value. We experimentally measured contrast values of ~0.9 with a very a similar stimulus and arena in previous experiments[46]. We used eight-level gray-scale interpolation to increase the apparent resolution of the system. In the 2-s intertrial period, we presented an evenly illuminated screen at mean luminance. For direction-tuning experiments (**Fig. 3**), we presented four repeats (blocks) of the eight directions of motion during nonflight and 1–4 blocks during flight. After flight, we presented 16 blocks of stimuli, the last four of which were averaged to generate the black curves in **Figure 3b**,**c**. For the time-course experiments (**Fig. 6**), we presented 20 stimuli before flight, 8–80 stimuli during flight and ≥80 stimuli after flight.

Preparation. The flight stage (**Fig. 1a**) was designed with Solidworks (Dassault Systèmes Solidworks) and milled out of Delrin plastic with a Roland MDX-650 (Roland DGA) computer-numerical control (CNC) mill. Flies were anesthetized on a Peltier device held near 4 °C and attached to the flight stage with ultraviolet-activated glue (Duro, Loctite) conventionally used in past experiments[9,46], and low melting–point wax. We clipped all six legs, or just the pro- and meso-thoracic legs, which promoted longer flight bouts. Because extension of the proboscis led to substantial brain movement, we glued the proboscis to the head capsule with a tiny drop of glue.

Once the fly was attached to the stage, we perfused the preparation with extracellular saline, removed a portion of cuticle and muscle number 1 with forceps, and approached the region of the brain overlying the VS cells with a micropipette (4–6-μm tip) containing 0.5 mg ml^{-1} collagenase IV (Worthington) in extracellular saline. Using positive pressure (40–80 mm Hg), we applied collagenase locally over the neural lamella for ~1–3 min, until we saw it rupture under 40× magnification. The collagenase digestion was conducted with the bath near 30 °C to accelerate enzymatic function; after rupturing the lamella, the bath temperature was lowered to 20 °C for the remainder of the experiment. As a final desheathing step, we used a micropipette to mechanically slice a portion of the exposed perineurial glia, revealing the VS-cell somas underneath. This combined enzymatic and mechanical protocol was adopted because mechanical desheathing with forceps alone would often tear out the very superficial VS-cell somas. Also, harsher proteases that were able to rupture both the collagen matrix of the neural lamella and the proteinaceous junctions of the perineurial sheath were found to leave the flies behaviorally unresponsive and unable to fly. All steps were conducted with infrared illumination and minimal use of epi-fluorescence so as to maintain the health of the fly.

We found that high-contrast images of the brain could be attained with diffuse illumination via adjustable light guides placed below the fly. This allowed us to removed the substage optics on the microscope (Nikon Eclipse FN1) and replace these with a camera that viewed the fly from below (see **Fig. 1**). We also used this camera for positioning the flies in the identical horizontal position across preparations. The precise head angle of flies could vary slightly across preparations; however, this was not a serious concern for these experiments because each individual had the identical field of view between flight and nonflight conditions. Also, we focused on wide-field stimuli that were likely to excite similarly large swaths of the receptive fields across individuals independent of the head angle. All recordings were made from cells on the right side of the brain.

Behavioral measurements. We recorded movies with a Prosilica GE680 camera attached to a fixed-focus Infinistix 90° lens (94-mm working distance, 1.0× magnification, Infinity). We illuminated the fly with infrared light (880 nm) directly from behind such that the wings generated a high luminance smear of reflected light in the captured image (**Supplementary Fig. 1**). An important kinematic parameter varied in tethered and freely flying flies is the peak downstroke angle achieved by the wing, or wing stroke amplitude[46,47]. Our goal was to estimate the wing stroke amplitude of the left and right wings so that we could observe the flies' steering responses during electrophysiological recordings.

Drosophila typically beat their wings at 180–250 Hz. We therefore captured images at 100 Hz (10 ms per frame, shutter open >9.8 ms each frame), ensuring that at least one full wing stroke, but no more than three, contributed to the contrast envelope generated by the moving wing in each analyzed image. For each frame, we generated a wing stroke amplitude measure for the left and right wings by means of the following algorithm (**Supplementary Fig. 1**). For each wing, we defined an analysis region as the area between two circular arcs, one with a larger radius than the other, centered on the wing hinge and overlying wing stroke plane. We divided this arcing region into multiple sectors (12 sectors are shown in the schematic of **Supplementary Fig. 1**) and on each frame we calculated the mean intensity of pixels enclosed by each sector. Because the background intensity was not uniformly low across the image (for example, notice the high-contrast white line cutting across the wing strokes in **Supplementary Fig. 1**), we subtracted from the intensity measure for each sector the background intensity value for that sector, measured before the fly started flying. We then plotted background-subtracted intensity measures for the left and right wings as a function of sector number. We linearly interpolated this function to achieve subsector resolution and found the location along the arcing region that had the midpoint intensity between the minimum and maximum intensity values observed on that frame. This location along the arcing region mapped directly to a wing-beat amplitude angle. This image-analysis algorithm was implemented as a plug-in for Motmot image-acquisition software[48]. We show estimates of wing-beat angle from an actual recording in **Supplementary Video 1**.

We found that wing-beat amplitude angles estimated in this manner yielded data similar in quality to those acquired previously with an optical wing-beat analyzer[28,46]. The principal difference between the methods is that the wing-beat analyzer provides wing stroke–by–wing stroke estimates of stroke amplitude, whereas the image-analysis method just described requires a small amount of stroke averaging. A benefit of the current method is that we obtain data directly in units of degrees, and a lengthy calibration of the optical wing-beat analyzer is avoided. We could not easily use the wing-beat analyzer with the current preparation because the flight stage scatters the infrared light source on its way from the emitter to the detectors, preventing a properly scaled shadow of the wings from falling on the detectors.

Solutions and electrophysiology. Our saline solutions were described previously[49]. The extracellular saline contained 103 mM NaCl, 3 mM KCl, 5 mM N-Tris(hydroxymethyl) methyl-2-aminoethanesulfonic acid, 10 mM trehalose, 10 mM glucose, 2 mM sucrose, 26 mM $NaHCO_3$, 1 mM NaH_2PO_4, 1.5 mM $CaCl_2$ and 4 mM $MgCl_2$ (pH 7.3 when equilibrated with 95% O_2 / 5% CO_2; 275 mOsm). Patch-clamp electrodes (4–7 MΩ) contained 140 mM potassium-aspartate, 1 mM KCl, 10 mM HEPES, 1 mM EGTA, 0.5 mM Na_3GTP, 4 mM MgATP and 13 mM biocytin hydrazide (pH 7.3, 265 mOsm). We also included 10–30 μM of Alexa 568–hydrazide-Na or Alexa 594–hydrazide-Na (most commonly 20 μM Alexa 568; Molecular Probes) in the intracellular solution to allow for immediate visualization of the cell's anatomy following experiments. For six cells, we did not include biocytin and observed no obvious differences in the physiological responses.

For voltage-clamp experiments, we compensated for whole-cell capacitance and for 50–70% of the series resistance. We held cells at −53 mV (near their typical resting potential) for 1 s between trials, stepped to −93 mV for 200–250 ms and then to voltages from −123 mV to −17 mV in 10-mV increments for 100 ms (**Fig. 4**). For each cell, we repeated the voltage steps three times before flight, three times during flight and four times after flight, waiting 5 min after the flight epoch ended until running the last three post-flight protocols. For one neuron, we only obtained a single repeat of the voltage steps in flight.

Voltage measurements have been corrected for a 13-mV, experimentally measured, junction potential. Current-clamp data were acquired at 10 or 20 kHz with Axoscope software (Molecular Devices) using an Axoclamp-2A (18 cells), Warner PC-501A (four cells) or an A-M Systems 2400 amplifier (56 cells). Voltage-clamp data were acquired at 30 kHz with winWCP software

doi:10.1038/nn.2492

(University of Strathclyde) using an A-M Systems 2400 amplifier (12 cells). All analyses were done with Matlab R2007b and R2009a (Mathworks).

We observed differences in the propensity of VS cells to fire full-blown action potentials across preparations, as was reported previously[12]. Approximately 10% of cells fired very large action potentials; however, these cells seemed no more or less likely to show the flight-dependent effects that we observed. For the majority of neurons (24 of 33) recorded in the direction-tuning experiment (**Fig. 3**), we did not inject hyperpolarizing current to influence V_m. The mean resting potential in neurons without current injection was −53 mV. For the remainder of neurons in the direction-tuning experiment and for all cells in the time-course experiments (**Fig. 6**), we injected tonic hyperpolarizing current, typically <50 pA, to bring the soma to a resting potential of −55 to −60 mV so as to compensate for the depolarizing effects of the leak conductance on small neurons[49,50]. We never adjusted the level of injected current during data acquisition. Note that the effects of flight in **Figures 3** and **6** did not differ appreciably and it is therefore unlikely that the modest amount of injected current had an influence on the results.

Anatomy and cell identification. For initial experiments, we visualized biocytin-filled neurons immunohistochemically. After recordings, we dissected brains, fixed in 4% formaldehyde (vol/vol) in phosphate-buffered saline for 15 min and blocked with 1:10 mouse nc82 (Developmental Studies Hybridoma Bank) and 1:250 rabbit antibody to GFP (Molecular Probes) overnight in PBST (phosphate-buffered saline and 0.2% Triton X-100) at 4 °C. After three washes for 20 min with PBST, we incubated the brains in 1:250 goat antibody to mouse:Alexa Fluor 633, 1:250 goat antibody to rabbit:Alexa Fluor 488 and 1:1,000 streptavidin:Alexa Fluor 568 overnight at 4 °C. After three washes for 20 min in PBST, we mounted brains in Vectashield, and took *z* stacks (1–2-μm slices) with either an LSM-510 confocal microscope (Zeiss) or a two-photon microscope (Prairie Technologies). The nc82 neuropil stain is not shown in **Figure 1c**,**d**.

In later experiments, we typically captured anatomical *z* stacks in wide-field fluorescence at 40× magnification *in vivo* using a moderately cooled CCD camera (Photometrics, CoolSnapEZ). At each *z* depth, we took a red-channel image of the Alexa 568– or Alexa 594–filled neuron and a green-channel image of the GFP-labeled VS cells. In the overlay of the red and green channels, we were able to identify VS1–6, as well as with immunohistochemically processed tissue. The quality of the epi-fluorescence images was high because the VS-cell dendrites are quite superficial.

We identified VS1–6 using anatomical criteria discussed in previous work[22]. In some direction-tuning experiments (20 of 33 cells in **Fig. 3**), however, we did not visualize the anatomy of filled cells. We confidently assigned a *post hoc* category of VS1–4 or VS5–6 to these original recordings by comparison with later data from unambiguously filled neurons. Specifically, VS5–6 typically depolarized to upward stimuli given the extent of our display, whereas VS1–4 typically hyperpolarized to these stimuli, particularly in flight. We also mapped receptive fields in all cells, with an upward and downward moving dot at 18 azimuthal positions, which facilitated identification. Note that all of the cells in **Figure 6** were categorized on the basis of their anatomy, not their physiological response, and these data show strong similarities to the data from **Figure 3**, in which 20 of 33 neurons were categorized on the basis of physiology alone.

Statistical analysis. Statistical comparisons used a two-tailed Student's *t* test.

45. Reiser, M.B. & Dickinson, M.H. A modular display system for insect behavioral neuroscience. *J. Neurosci. Methods* **167**, 127–139 (2008).
46. Maimon, G., Straw, A.D. & Dickinson, M.H. A simple vision-based algorithm for decision making in flying *Drosophila*. *Curr. Biol.* **18**, 464–470 (2008).
47. Fry, S.N., Sayaman, R. & Dickinson, M.H. The aerodynamics of free-flight maneuvers in *Drosophila*. *Science* **300**, 495–498 (2003).
48. Straw, A.D. & Dickinson, M.H. Motmot, an open-source toolkit for real-time video acquisition and analysis. *Source Code Biol. Med.* **4**, 5 (2009).
49. Wilson, R.I. & Laurent, G. Role of GABAergic inhibition in shaping odor-evoked spatiotemporal patterns in the *Drosophila* antennal lobe. *J. Neurosci.* **25**, 9069–9079 (2005).
50. Barry, P.H. & Lynch, J.W. Liquid junction potentials and small-cell effects in patch-clamp analysis. *J. Membr. Biol.* **121**, 101–117 (1991).